UCRL-ID-143328

Evaluation of the ^{239}Pu(n, 2n) Integrated Cross Section

D. P. McNabb, J. D. Anderson, R. W. Bauer, J. A. Becker, F. Dietrich, P. Navratil, M. B. Chadwick, and P. G. Young

January 25, 2001

U.S. Department of Energy

Lawrence Livermore National Laboratory

DISCLAIMER

This work was performed under the auspices of the U. S. Department of Energy by the University of California, Lawrence Livermore National Laboratory under Contract No. W-7405-Eng-48.

Evaluation of the ^{239}Pu$(n, 2n)$ integrated cross section

D. P. McNabb, J. D. Anderson, R. W. Bauer, J. A. Becker, F. Dietrich, P. Navratil
LLNL
M. B. Chadwick, P. G. Young
LANL

January 25, 2001

Contents

1 Introduction **3**

2 Evaluation of ^{239}Pu$(n, 2n)$ measurements **5**
2.1 Lougheed *et al.* activation measurement 6
2.1.1 Summary 6
2.1.2 Determination of the neutron fluence, average energy, and energy spread 8
2.1.3 Summary of evaluated results and uncertainties 13
2.2 Frehaut *et al.* and Mather *et al.* direct neutron-counting measurements 13
2.2.1 Summary 13
2.2.2 Required corrections and estimate of systematic uncertainties 17
2.2.3 Summary of evaluated results and uncertainties 17
2.3 GEANIE partial gamma-ray measurement 18
2.3.1 Partial cross section results summary 20
2.3.2 Reaction model results summary 20
2.3.3 Summary of evaluated results and uncertainties 23

3 Consistency with other experimental data **25**
3.1 Shape of the $(n, 2n)$ cross section 25
3.2 Magnitude of the $(n, 2n)$ cross section 27
3.2.1 σ_{non} constraint 29
3.2.2 $\sigma_{(n,n')}$ constraint 30

4 Recommended ^{239}Pu$(n, 2n)$ cross section and uncertainties **32**

5 Acknowledgements **36**

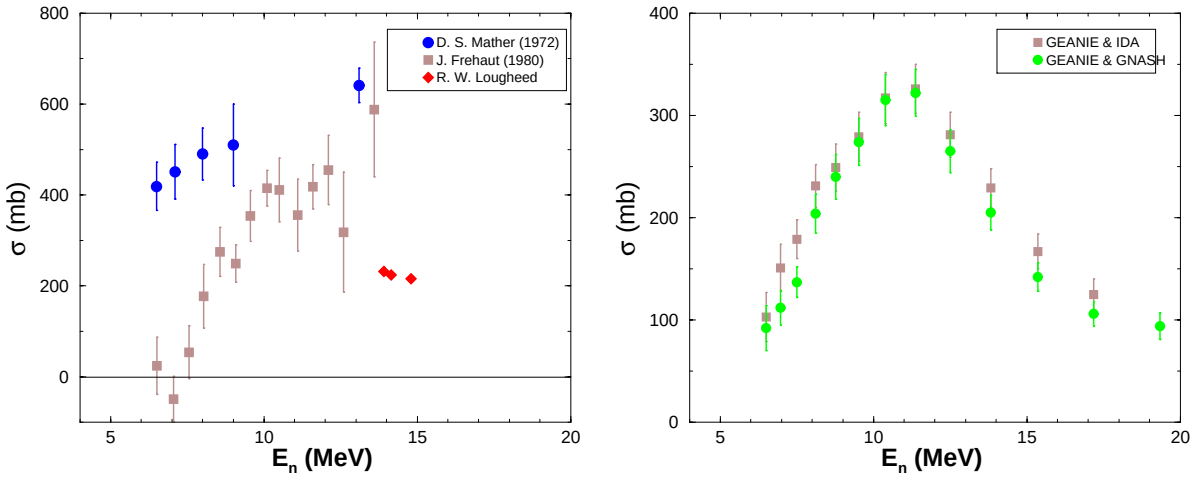

(a) (b)

Figure 1: A summary of available ^{239}Pu$(n, 2n)$ cross section data. (a) The ^{239}Pu$(n, 2n)$ data circa 1985. (b) The ^{239}Pu$(n, 2n)$ cross section as inferred by Bernstein *et al.* [Ber00] using nuclear model calculations of Chen *et al.* [Che00] (IDA) and Chadwick *et al.* [Cha99] (GNASH00).

1 Introduction

Recently, new cross section measurements by the GEANIE collaboration (for overview see Becker *et al.* [Bec01]) have been published for ^{239}Pu$(n, 2n\gamma)$ [Ber00] and ^{235}U$(n, 2n\gamma)$ [You00] from threshold to 20 MeV. When combined with nuclear reaction calculations [Che00, Cha99, Cha01], these measurements provide the most accurate information available on the shape and magnitude of the ^{239}Pu$(n, 2n)$ cross section for incident neutron energies, $E_n \lesssim 14$ MeV. This new data has prompted a re-evaluation of the ^{239}Pu$(n, 2n)^{238}$Pu reaction cross section considering all available experimental data.

The data prior to the measurement of Bernstein *et al.* [Ber00] is illustrated in Figure 1a. These data sets were considered by previous evaluations [ENDL] of the ^{239}Pu$(n, 2n)$ cross section. The most precise experiment was an activation measurement done by Lougheed *et al.* [Lou00][1] for incident neutron energies, E_n, between 13-15 MeV. In addition, there were two neutron-counting experiments, one by Mather *et al.* [Mat72] and one by Frehaut *et al.* [Fre85]. These two measurements cover a wide incident neutron range, with data points from threshold to $E_n \approx 14$ MeV. The available data sets are in poor agreement with each other and in some cases do not meet basic expectations. These experiments will be reviewed in detail.

The new contributions to this evaluation are (1) the GEANIE data coupled with reaction modeling, illustrated in Figure 1b, and (2) the systematic use of other nuclear data in order to put constraints on the shape and magnitude of the ^{239}Pu$(n, 2n)$ cross section. The approach

[1]The Lougheed *et al.* measurement was available in 1985 and was privately communicated to the authors of this evaluation in 2000.

of this evaluation has been to use consistency arguments supported by nuclear data to resolve the measurement differences, with the goal of providing:

- A comprehensive picture of our knowledge on the ^{239}Pu$(n, 2n)$ cross section
- A new evaluation including the best possible estimate of the cross section and a one-sigma estimate the uncertainties

This paper is organized in the following fashion:

Section 2: Evaluation of ^{239}Pu$(n, 2n)$ measurements Measurements of the ^{239}Pu$(n, 2n)$ cross section are evaluated for reliability (systematic uncertainties) and for renormalization possibilities.

Section 3: Consistency with other experimental data Experimental data and nuclear data evaluations for non-elastic, inelastic, fission, $(n, 2n)$, and neutron production cross sections are reviewed in the context of unitarity and other constraints. Conclusions with regard to the shape and magnitude of the ^{239}Pu$(n, 2n)$ cross section are drawn.

Section 4: Recommended ^{239}Pu$(n, 2n)$ cross section and uncertainties The results of Section 2 and 3 are combined to provide an overall "best" data set with evaluated uncertainties. The recommended ^{239}Pu$(n, 2n)$ cross sections and relative uncertainties are given in tabular format and compared with other evaluations.

2 Evaluation of ^{239}Pu$(n, 2n)$ measurements

Three distinct techniques have been used to measure $(n, 2n)$ reaction cross section in actinide nuclei:

Activation: Counting radioactivity emitted by residual nuclei after neutron irradiation of the target.

Neutron counting: Counting the number of events for which two neutrons are promptly emitted in excess of the number of emitting two neutrons during fission.

Partial γ rays: Counting the prompt emission of γ rays characteristic of the residual nucleus (^{238}Pu), coupled with nuclear modeling to infer the cross section of the $(n, 2n)$ channel.

In this Section, measurements of the ^{239}Pu$(n, 2n)$ cross section are evaluated for reliability (systematic uncertainties) and for renormalization possibilities. The measurements made with each technique are considered in turn.

The evaluation of the activation measurement by Lougheed *et al.* [Lou00] for incident neutron energies, E_n, between 13-15 MeV is discussed in Section 2.1. This is the most precise measurement of the magnitude of the ^{239}Pu$(n, 2n)$ cross section. Most of the systematic uncertainty in this measurement arises in the determination of the neutron fluence, so special attention is given to the magnitude and energy dependence of the neutron fluence. In this evaluation, the magnitude of the neutron fluence has been renormalized by $1 - 2\%$ and the average neutron energies quoted for each data point have been modified to be in agreement with direct experimental data rather than from Monte Carlo simulations.

The evaluation of the neutron counting measurements by Frehaut *et al.* [Fre85] and Mather *et al.* [Mat72] for $6 < E_n < 14$ MeV is discussed in Section 2.2. Mather *et al.* were pioneers in the sense that their measurements were the first attempt to use the direct neutron counting technique with fissionable isotopes. The Mather *et al.* data has been rejected in this evaluation because (1) the data is inconsistent with other nuclear data in ^{239}Pu as discussed in Section 3 and (2) the experiment lacked good information on the low-energy neutron fluence, which draws into question the ability of Mather *et al.* to properly subtract the background fission neutrons. Frehaut *et al.* made some improvements to the technique in determining the nature of the neutron background. As a result, Section 2.2 focuses on the Frehaut *et al.* experiment. However, the Frehaut *et al.* data was not used in determining the evaluated cross section in Section 4 for three reasons: (1) the energy-dependent uncertainties are large, particularly at higher incident energies, (2) the data do not rise at threshold with increasing E_n as expected based on simple theoretical arguments put forth in Section 3.1, and (3) the difficulties encountered when using the ^{239}Pu sample may lead to additional systematic uncertainties not considered in this evaluation. It should be noted that the Frehaut *et al.* data is consistent with the evaluated results of Section 4.

The evaluation of the partial gamma-ray cross-section measurements by the GEANIE collaboration (Becker *et al.* [Bec01], Bernstein *et al.* [Ber00]) is discussed in Section 2.3 for $E_n < 20$ MeV. This measurement provides a direct lower limit to the ^{239}Pu$(n, 2n)$ cross section on a stand alone basis, as well as shape and magnitude information when coupled with the

results of nuclear reaction modeling. Because systematic uncertainties are not strongly E_n-dependent, this combination of measurement and theoretical interpretation provides the best information available on the shape of the ^{239}Pu$(n,2n)$ cross section. Special attention in this evaluation is given to the sensitivity of the shape to the nuclear reaction modeling.

2.1 Lougheed *et al.* activation measurement

2.1.1 Summary

Lougheed *et al.* [Lou00] irradiated high-purity ^{239}Pu samples with neutrons at the LLNL ICT facility [Won72] using the rotating target assembly. The $t(d,n)\alpha$ reaction was employed to obtain a high integrated flux ($\approx 10^{12}$ n/s) of $E_n \approx 14$ MeV neutrons. A schematic of the Lougheed measurement is depicted in Figure 2. A high-current (≈ 100 mA), 400 keV deuteron beam is incident on a substrate-supported TiT_2 target. The deuterium fuses with the tritium producing a high flux of 14 MeV neutrons that irradiate the sample foils. Four "detector" packages were placed at different angles with respect to the incident deuteron beam, but only the downstream package is pictured in Figure 2. The detector package include Fe and Au foils with the Pu samples. The Fe and Au foils were used to measure the average neutron energy, E_n, and the neutron fluence Φ_n. The angular positions of the four detector packages were chosen such that the nominal values of E_n were 13.8, 14.0, 14.6, and 14.8 MeV. The irradiation lasted for about six days.

The number of ^{238}Pu atoms produced, N_{238}, is given by

$$N_{238} = N_{239}\Phi_n\sigma_{(n,2n)} \tag{1}$$

where N_{239} is the number of ^{239}Pu atoms in the sample, Φ_n is the fluence of neutrons incident on the sample, and $\sigma_{(n,2n)}$ is the ^{239}Pu$(n,2n)$ cross section. The neutron fluence was determined by measuring γ rays produced by activation of the gold foils via the ^{197}Au$(n,2n)^{196}$Au reaction of known ($\approx 2\%$) cross section. An proton-recoil monitor allowed corrections for time fluctuations of the neutron flux which arise from fluctuation in the deuteron beam intensity and the depletion of tritium in the target. The mean neutron energy was determined by measuring γ rays following activation of the iron foils via the ^{54}Fe(n,p) reaction of known ($\approx 3\%$) cross section. The number of plutonium atoms, N_{238} and N_{239}, are determined from the number of α decays, A, of these nuclei weighted by their decay rates, λ, *e.g.*

$$N_{238} \propto \frac{A_{238}}{\lambda_{238}}. \tag{2}$$

After irradiation, the plutonium samples were dissolved and then deposited in a thin layer on a substrate so that no correction needs to be made for the attenuation of the α radiation in the sample. The α-decay of ^{239}Pu ($Q_\alpha = 5.244$ MeV) is easily resolvable from the α-decay of ^{238}Pu ($Q_\alpha = 5.593$ MeV) with the silicon surface-barrier detector used to count the α activity; both α-decay groups are detected with the same efficiency. The ratio of α decay in ^{238}Pu to

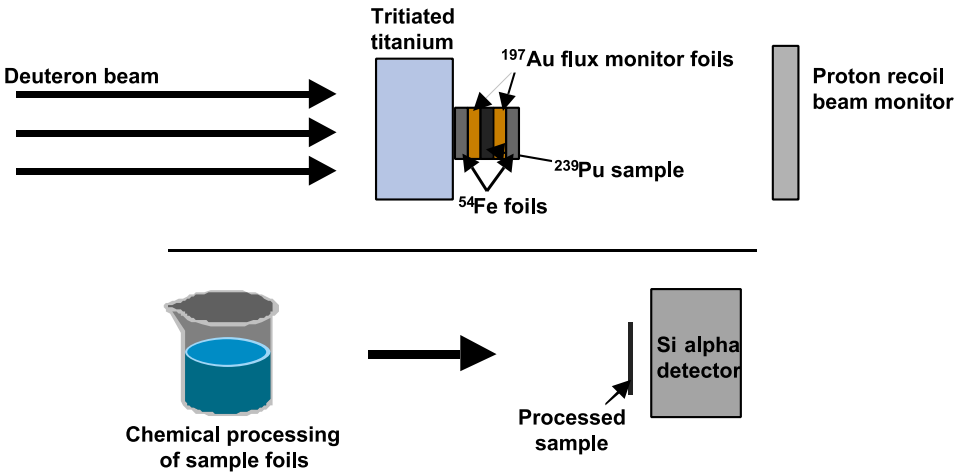

Figure 2: A schematic of the Lougheed *et al.* activation measurement [Lou00].

^{239}Pu, A_{238}/A_{239}, is measured with high precision over the course of several months.[2]

In the limit that the mean-life of ^{238}Pu, $\tau_{238} = 1/\lambda_{238}$, is much longer than the counting time or irradiation time, then the $(n, 2n)$ cross section is given by:

$$\sigma_{(n,2n)} \approx \frac{1}{\Phi_n} \frac{\lambda_{239}}{\lambda_{238}} \frac{A_{238}}{A_{239}} \tag{3}$$

where Φ_n is the neutron fluence. This approximate equation is used for discussion in this evaluation, but an exact integral equation was used by Lougheed. It is clear from Equation 3, however, that $\sigma_{(n,2n)}$ is independent of both the plutonium sample mass and the α detection efficiency. Since the decay rates of ^{239}Pu and ^{238}Pu are known to better than 1%, there is no likely source of significant systematic uncertainty in the determination of N_{238}/N_{239}. However, a similar cancellation does not occur in the determination of Φ_n. For this reason, this evaluation focuses on obtaining a detailed understanding of Φ_n — the systematic uncertainties in its magnitude, average energy, and energy spread.

2.1.2 Determination of the neutron fluence, average energy, and energy spread

Activation foils from which the neutron fluence ^{197}Au and its average energy (^{54}Fe) were deduced are depicted in the detector package shown in Figure 2. The ^{197}Au foils were used to obtain the neutron fluence and the ^{54}Fe foils determined the average neutron energy using the radio-activation technique described in [ASTM]. The neutron beam energy profile was not measured in-beam, but was determined from Monte Carlo transport models.

The ^{239}Pu$(n, 2n)$ cross section is decreasing rapidly at $E_n = 14$ MeV; it has a slope of about 50 mb/MeV according to the GEANIE data discussed in Section 2.3. Therefore, a small uncertainty in the average incident neutron energy translates into a large uncertainty in the quoted cross section. The uncertainty in the average incident energy is one of the largest contributions to the uncertainty of the Lougheed data points.

Neutron fluence

The neutron fluence, Φ_n, was measured via the ^{197}Au$(n, 2n)^{196}$Au reaction. The half-life of ^{196}Au is 6.183 days, approximately equal to the irradiation time. ^{196}Au β^+-decays to ^{196}Pt 92.5(5)% of the time. Subsequent decay γ-rays were observed with a calibrated ($\approx 2\%$) germanium detector, a detector with precision energy resolution and excellent response function. The advantages of this particular standard are (1) the ^{197}Au(n,2n) cross section is essentially flat from about 11 MeV to 15 MeV (the ^{197}Au$(n, 3n)$ channel opens at 14.8 MeV) and (2) gold is mono-isotopic. The neutron beam was monitored with a proton-recoil telescope to account for time variations of the neutron flux, $\phi_n(t)$.

[2] An aside: The nominally 14.6 MeV data point was rejected by Lougheed because it was 20 standard deviations larger than the other data points. Lougheed believes that the sample in this package was contaminated during the chemical processing of the plutonium. This scenario does not invalidate the other data points (see Figure 1a). Contamination can only increase experimentally-determined cross sections and it does not seem likely that essentially equal amounts of ^{238}Pu contamination were present on the other three samples.

The neutron fluence, Φ_n, is given by

$$\Phi_n = \frac{A}{\varepsilon_{det}\sigma_{\mathrm{Au}(n,2n)}N_{\mathrm{Au}}} \times \frac{\int_{t_1^i}^{t_2^i} \phi_n(t)\,dt}{\int_{t_1^i}^{t_2^i} \phi_n(t)e^{-\lambda t}\,dt} \times \frac{t_2^c - t_1^c}{e^{-\lambda t_2^c} - e^{-\lambda t_1^c}} \tag{4}$$

where A is the number of ^{196}Au γ-ray decays observed (corrected for branching ratio), ε_{det} is the detection efficiency, t_1^i and t_2^i are the times beginning and ending the irradiation, and t_1^c and t_2^c are the times beginning and ending the off-line counting.

The main sources of systematic uncertainty in Φ_n are ε_{det} and $\sigma_{^{197}\mathrm{Au}(n,2n)}$. The uncertainty in ε_{det} is taken to be 2%. The best previous evaluations of the $\sigma_{^{197}\mathrm{Au}(n,2n)}$ were done by Ryves [Ryv89] and Wagner *et al.* [Wag90]. Ryves reports a simultaneous evaluation of twelve of the best known cross sections at 14.7 MeV. Wagner *et al.* evaluates the shape of the $^{197}\mathrm{Au}(n,2n)$ cross section from threshold to 30 MeV and normalizes to Ryves at 14.7 MeV. Since these evaluations were completed, there have been five new measurements of $\sigma_{^{197}\mathrm{Au}(n,2n)}$ between 13-15 MeV. These measurements are in excellent agreement with the shape evaluated by Wagner *et al.* Table 1 summarizes these five new measurements and the Ryves value at 14.7 MeV. A comparison of the quoted uncertainties with the distribution of the five recent measurements suggests that the systematic uncertainties of these recent measurements have been underestimated. A simple average of the five recent measurements gives a cross section value of 2064(64) mb, in good agreement within errors with the Ryves value of 2127(26) mb. Since the Ryves value and Wagner *et al.* shape were determined in a careful and consistent manner, these values have been adopted for this evaluation, rather than attempt to fold the five recent measurements into the evaluation. Table 2 compares the Wagner *et al.* evaluated cross sections and relative uncertainties for $\sigma_{^{197}\mathrm{Au}(n,2n)}$ between 13-15 MeV with the values used by Lougheed *et al.*. The uncertainties given by Wagner *et al.* have been increased to account for a systematic uncertainty (1%) in the γ-ray decay branching ratio, which is not accounted for by either Ryves or Lougheed *et al.*. The Wagner *et al.* results and revised uncertainties, as listed in Table 2, have been adopted for this evaluation. The Lougheed values have been renormalized accordingly, and the uncertainties propagated.

Table 1: Summary of reports regarding the normalization the ^{197}Au$(n,2n)$ cross section at 14.7 MeV.

Data source	$\sigma_{^{197}\mathrm{Au}(n,2n)}$ (mb)	Method; Normalization
Ryves [Ryv89]	2127(26)	Simultaneous evaluation
Ikeda [Ike88]	1894(97)	γ-ray activation w/Ge; ^{27}Al(n,α)
Kobayashi [Kob88]	2140(79)[3]	γ-ray activation w/Ge; ^{27}Al(n,α)
Wang [Wan89]	2147(114)	γ-ray activation w/unknown; ^{27}Al(n,α)
Garlea [Gar92]	1896(85)	γ-ray activation w/Ge; ^{93}Nb$(n,2n)$
Filatenkov [Fil99]	2242(90)	γ-ray activation w/Ge; ^{93}Nb$(n,2n)$

Table 2: ^{197}Au$(n,2n)$ cross sections adopted in this evaluation compared with values used by Lougheed *et al.*.

E_n MeV	$\sigma_{^{197}\mathrm{Au}(n,2n)}$ (mb)	Relative uncertainty	[Lou00] value
13.45	2101.3	0.016	-
13.75	2111.5	0.016	2153
14.00	2112.0	0.016	2157
14.25	2123.9	0.016	2160
14.50	2123.5	0.016	2160
14.75	2135.5	0.017	2160
15.00	2134.7	0.028	2160

Average energy

The average energy of each irradiation was determined with the ^{54}Fe$(n,p)^{54}$Mn reaction. The β-decay of ^{54}Mn has a half-life of 312.12 days, and results in a 835 keV γ-ray with a 99.975% branching ratio. The advantages of this particular standard are (1) the cross section varies linearly with a large slope for E_n between 13 and 15 MeV, decreasing by 40% over this energy range, (2) the half-life and decay properties make these samples easy to handle and

[3]Measurement at $E_n = 14.1$ MeV. Increased measured value by 15 mb, consistent with evaluated shape, in order to determine value at $E_n = 14.7$ MeV.

count, and (3) the cross section is known to 3%. By comparing the production yield of ^{54}Mn, which varies with E_n, to the production yield of ^{196}Au, which is constant with E_n, the average energy of the irradiation is determined.

The measured production cross section for ^{54}Mn is associated with the average energy of the irradiation. The best evaluation available for the $^{54}\mathrm{Fe}(n,p)^{54}\mathrm{Mn}$ standard was done by Fu [Fu82], and is part of ENDF-B/VI. The work of Fu was a simultaneous evaluation of 12 dosimetry reactions in the 13-15 MeV energy region. Table 3 summarizes the relevant data from this evaluation. Fu recommends a 3% 1-sigma uncertainty for this standard. Other sources of uncertainty in the determination of the ^{54}Mn production include statistical uncertainties and systematic uncertainties in Φ_n.

Table 3: Recommended $^{54}\mathrm{Fe}(n,p)^{54}\mathrm{Mn}$ cross sections [Fu82]. An overall uncertainty of 3% is recommended.

E_n MeV	$\sigma_{^{54}\mathrm{Fe}(n,p)}$ (mb)
13.00	410
13.50	383
14.00	342
14.50	306
15.00	270

Lougheed *et al.* have quoted nominal beam energies in data releases, and not the average beam energies determined from the Fe and Au detector foils. Table 4 gives the average beam energies determined from $^{54}\mathrm{Fe}(n,p)^{54}\mathrm{Mn}$ and the nominal beam energies used by Lougheed *et al.* Lougheed *et al.* expressed concern to us with the 0.27 MeV difference between the nominal value of 14.8 MeV for the forward irradiation, and the value of 14.53 MeV determined from the ^{54}Mn data. We have decided to rely on the average energy of irradiation derived from the ^{54}Mn production because these values are experimentally determined, can be clearly stated, and are amenable to uncertainty analysis. We do not believe the 0.27 MeV discrepancy to be unreasonable, given the close geometry as discussed below in the section on beam energy profile. Table 4 summarizes the average energy of irradiation determined from the ^{54}Mn production data and evaluated uncertainties.

Table 4: The ^{54}Mn production cross section reported by Lougheed *et al.* is summarized for all three data points. The average energy of irradiation determined from this cross section and Table 3 is also given. The uncertainties in the average energies are quoted in parentheses, and the resulting uncertainty in the $^{239}\mathrm{Pu}(n,2n)$ cross section assumes that the $^{239}\mathrm{Pu}(n,2n)$ cross section is decreasing at 50 mb/MeV.

Nominal E_n (MeV)	$\sigma_{^{54}\mathrm{Fe}(n,p)}$			Average E_n (MeV)	Resulting relative uncertainty in $^{239}\mathrm{Pu}(n,2n)$ cross section
	Value (mb)	Relative systematic uncertainties	Relative statistical uncertainties		
13.8	349.1	0.039	0.010	13.91(20)	0.042
14.0	330.9	0.039	0.010	14.15(19)	0.042
14.8	302.5	0.039	0.010	14.53(17)	0.040

Beam energy profile

The experiment of Lougheed *et al.* was done in a very close geometry. For example, the sample nominally irradiated at $E_n = 14.8$ MeV sample was 6.35 mm in diameter, located about 3.3 mm directly downstream of the beam-target interaction point. The tritiated titanium target is thick enough to stop the deuteron beam, so the neutron spectrum irradiating the target is an energy and angle integration over the incident deuterons slowing down in the target with energies from 0 to 400 keV, and over the solid angle subtended by the sample foils, which is essentially from 0° to 45° for the nominal 14.8 MeV sample. The mean neutron energy at 0° is 15.1 MeV, and the mean neutron energy at 90° is 14.1 MeV. The neutron intensity is anisotropic at the 10-15% level over this angular range. Thus, while this close geometry substantially increased the neutron fluence, the large solid angle subtended by the sample broadens the neutron beam energy to about 400-keV FWHM. The samples located at other angles were further from the interaction point and so the incident neutron energies are not as broadened. There is one more point to note: an important advantage of such a close geometry is that the fraction of incident neutrons interacting with the sample that arise from scattering off distant materials, such as the room walls, is small relative to the incident neutron fluence.

2.1.3 Summary of evaluated results and uncertainties

The evaluated data of Lougheed *et al.* together with statistical and systematic uncertainties are summarized in Table 5. The average energies of irradiation are taken to be the values determined from the ^{54}Mn production; for example, the highest energy data point has been changed from the nominal value of 14.8 MeV to the measured value of 14.53(17) MeV. The magnitude of the data points have been scaled up by $\approx 1.5\%$ to reflect the change in the values used for $^{197}\mathrm{Au}(n,2n)$ cross section. The uncertainties of the incident neutron energies reflect the uncertainties in the average energy only. The uncertainties do not include the neutron beam energy spread, because to an excellent approximation, the $^{239}\mathrm{Pu}(n,2n)$ cross section varies linearly over the the neutron beam energy spread of about ± 300 keV. Therefore, the spread in the incident neutron energy has negligible effect on the quoted cross section values.

The systematic uncertainties include the uncertainty in the $^{197}\mathrm{Au}(n,2n)$ cross section listed in Table 2, as well as a 2% uncertainty assumed for the γ-ray counter efficiency. The statistical uncertainties are from Lougheed *et al.* and they include counting statistics in the determination of the average energy, flux normalization, and the area of the α-decay peaks due to ^{238}Pu and ^{239}Pu.

Table 5: The Lougheed ^{239}Pu $\sigma_{(n,2n)}$ data values and relative statistical and systematic uncertainties used in this evaluation. The combined uncertainty includes the uncertainty in the average neutron energy under the assumption that the cross section is decreasing at a rate of 50 mb/MeV.

$\bar{E}_n$ (MeV)	$\sigma_{(n,2n)}$ (mb)	Relative uncertainties		
		Statistical	Systematic	Combined
13.91(19)	237	0.040	0.047	0.062
14.15(18)	228	0.022	0.047	0.052
14.53(17)	220	0.015	0.047	0.049

2.2 Frehaut *et al.* and Mather *et al.* direct neutron-counting measurements

2.2.1 Summary

The experimental setup used by Frehaut *et al.* is schematically depicted in Figure 3. A pulsed, collimated neutron beam is incident on the ^{239}Pu sample. The number of emitted or scattered neutrons is detected in a large, gadolinium-loaded liquid scintillator ($\approx 80\%$ efficient). The scintillator relaxation time is about 30 μs. Two-neutron events are distinguished in this

arrangement by taking advantage of the relaxation time in the scintillator.

The basic idea behind neutron counting measurements is to detect the number of two-neutron events due to the $(n, 2n)$ reaction apart from scattered and fission neutrons. In cases where there is no fission, the number of two-neutron events is proportional to the (n,2n) cross section. However, with fissionable nuclei one must determine the number of two-neutron events in excess of the number of two-neutron fission events. Hence the cross section is given by

$$\frac{\sigma_{(n,2n)}}{\sigma_{(n,f)}} = \frac{N(2) - N_f P_f(2)}{N_f} \tag{5}$$

where $N(2)$ is the number of two-neutron events, N_f is the number of fission events, and $P_f(2)$ is the probability that fission resulted in two neutrons being emitted. Below the $(n, 3n)$ threshold, events with three or more neutrons can only arise from fission events. By using the fission neutron distribution, $P_f(\nu)$, which has been independently measured, the number of fission events, N_f, can be deduced from the number of three- and higher-neutron fission events using the following equation:

$$N_f = \frac{\sum_{m \geq 3} N(m)}{\sum_{\nu \geq 3} P_f(\nu)} \tag{6}$$

There are several difficulties with this technique for measuring the ^{239}Pu$(n, 2n)$ cross section:

1. The ^{239}Pu$(n, 2n)$ cross section is small relative to the fission cross section, and therefore, the numerator of Equation 5 is the difference of two large numbers. The resulting error propagation limits the statistical accuracy of this technique.

2. Random background rates are high due to the high γ-ray activity of ^{239}Pu and the spontaneous fission neutron activity of ^{240}Pu. This background also hurts the statistical accuracy of the measurement.

3. In-beam false coincidence rates are high because of the large-angle elastic scattering of neutrons on the aluminum cladding. This was corrected on the basis of the number of single neutron events observed.

4. ^{239}Pu is thermally fissile, and therefore, fission events also arise from beam-related low-energy neutrons ($E_n < 550$ keV). Corrections for this effect vary with incident neutron energy.

5. The large plutonium sample results in several multiple scattering corrections. Incident neutrons can be down-scattered before inducing an $(n, 2n)$ or (n, f) event. Emitted neutrons can also be absorbed in the sample, often inducing another fission.

6. The scintillator detection efficiency was determined for fission neutrons. The detection efficiency for the $(n, 2n)$ neutron spectrum has been modeled to be higher, resulting in a -9% correction to $\sigma_{(n,2n)}$.

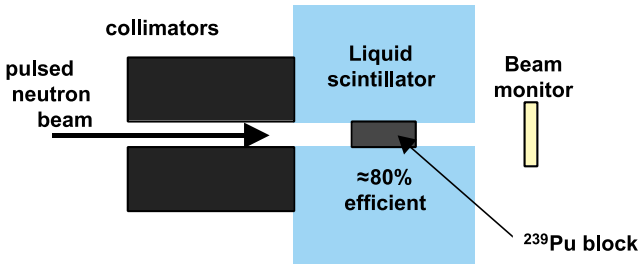

Figure 3: A schematic of the Frehaut *et al.* neutron counting measurement [Fre85].

Uncertainties arising from Items 1-3 above are statistical in nature and are represented in the uncertainties quoted by Frehaut *et al.* Frehaut *et al.* also incorporate the estimated uncertainty in $P_f(\nu)$ in the data analysis. Estimates of systematic uncertainties inherent in Items 4-6, as well as systematic uncertainties in the normalization standards, are discussed below in Section 2.2.2. These systematic uncertainties are not reflected in the Frehaut *et al.* data, but are in this evaluation.

Some particular details of the Frehaut *et al.* and Mather *et al.* measurements are summarized below, followed by a discussion of systematic uncertainties.

Frehaut *et al.* particulars

The plutonium sample consisted of 15.5 g of 99.87% enriched metallic ^{239}Pu. The remainder of the sample was ^{240}Pu. The sample was clad in 0.3 mm of aluminum and encapsulated in a 0.3 mm thick aluminum can. The neutrons were produced with either the $t(p,n)^3He$ or $d(d,n)^3He$ reaction, using a 10 cm long gaseous target. The beam was pulsed at a frequency of 2.5 MHz (pulse spacing of 400 ns) and an electrostatic beam sweeper was used to keep three proton/deuteron pulses every 60 μs. The proton/deuteron pulse width was about 2 ns. The incident neutron energy spectrum was monitored with the time-of-flight technique using a small liquid scintillator 4 m from the gas target. The relative detection efficiency of the neutron monitor was determined with a ^{252}Cf spontaneous fission source and Monte Carlo code calculations to account for different neutron energy spectra. This system allowed Frehaut *et al.* to measure the relative incident neutron fluence for $E_n > 550$ keV.

Mather *et al.* particulars

The experimental setup of Mather *et al.* is very similar to Frehaut *et al.* The Mather *et al.* data has been rejected in this evaluation because (1) the Mather *et al.* data is inconsistent with other nuclear data in ^{239}Pu as discussed in Section 3 and (2) the lack of good information on the low-energy neutron fluence and the unphysical value near threshold suggests that Mather *et al.* did not properly subtract off the background fission neutrons. In fact, the large cross section values and small statistical error bars on the Mather *et al.* data points near threshold, shown in Figure 1, likely result from an undersubtraction of the fission neutron background. Therefore, some particulars of the Mather *et al.* experiment are summarized here for pedagogical reasons, and are not explored further.

The plutonium sample consisted of two 3.95 g/cm^2 metallic disks clad in 0.25 mm of aluminum. The sample was 99.4% enriched ^{239}Pu, with the remaining 0.6% being ^{240}Pu. The neutrons were produced using the $d(d,n)^3He$ reaction for $E_n < 9$ MeV and using the $t(d,n)\alpha$ reaction for $E_n > 12$ MeV. The Van de Graaff accelerator was limited to a 6 MeV terminal voltage, which meant that neutrons with $9 < E_n < 12$ were not accessible. The deuterons were pulsed at a frequency of 9 kHz (pulse spacing of 110 μs) and had a pulse width of about 1 μs. The $E_n > 12$ MeV measurements employed a 2.5 mg/cm^2 titanium tritide target. The collimator/detector system was rotated to different angles with respect to the beam and the incident beam energy was varied to achieve different incident neutron energies when the titanium tritide target was used. The relatively thin titanium tritide provided a neutron energy spread of about 200 keV. For the lower energy data points, the collimator/detector arrangement was aligned at

5°. The deuteron energy loss in the entrance windows resulted in an energy spread of about 100 keV in E_n.

Mather *et al.* did not have an in-beam neutron fluence monitor, but made a 30% correction to neutron fluence for the 13.1 MeV data point based on a separate fission chamber measurement. No other corrections for the presence of low-energy neutrons were made.

2.2.2 Required corrections and estimate of systematic uncertainties

Frehaut *et al.* discusses the corrections made for low-energy beam-related neutrons, multiple scattering, and the $(n, 2n)$ neutron detection efficiency in a description of the ^{235}U$(n, 2n)$ cross section measurement [Fre80]. They estimate the uncertainty in these corrections to be between 5-7%. Because the larger (n, f) cross section in ^{239}Pu increases the magnitude of some of these corrections, this evaluation adopts the high-end value of 7%. The actual uncertainty may be larger, but the information needed to make an accurate estimate of the uncertainty is not available.

Frehaut *et al.* calibrated the efficiency of the neutron detector with a ^{252}Cf source. They used the value $\bar{\nu} = 3.733$. The current value is approximately 1% larger: $\bar{\nu} = 3.7676(49)$ [Car93]. This new value of $\bar{\nu}$ implies that the efficiency for detecting a single neutron should be decreased by $\approx 1\%$, and therefore, changes the values $N(m)$ derived by Frehaut *et al.* during the data analysis. Using Equations 5 and 6, the Soleilhac *et al.* [Sol69] values for $P_f(\nu)$, and an approximate fission cross section of 2 barns, we derive a first-order correction of -2.5%. Second-order effects, which arise when determining background rates due to falsely coincident events and events with unobserved neutrons, cannot be determined without the raw data. Hence, in this evaluation, the Frehaut *et al.* data points and statistical uncertainties have been scaled down by 2.5%.

2.2.3 Summary of evaluated results and uncertainties

The renormalized Frehaut *et al.* data and the statistical and systematic uncertainties ascribed to the data in this evaluation are summarized in Table 6. As discussed above, the magnitude of the Frehaut *et al.* data points has been scaled down by 2.5% to reflect the change in the accepted value of $\bar{\nu}$ in ^{252}Cf. The statistical uncertainties are taken from [Fre85] and the systematic uncertainties (7%) are taken from [Fre80], as discussed in Section 2.2.2. The neutron beam energy spread is nominally ± 50 keV due to energy loss in the gas target. This energy spread together with any uncertainty in the average energy of the beam is neglected in this evaluation.

Table 6: ^{239}Pu $\sigma_{(n,2n)}$ data values and statistical and systematic uncertainties evaluated from Frehaut *et al.* A small renormalization and the relative systematic uncertainties assumed are discussed in the text.

E_n (MeV)	$\sigma_{(n,2n)}$ (mb)	Statistical uncertainties (mb)	Systematic uncertainties (mb)	Combined uncertainty (mb)
6.49	23	61	2	61
7.01	-48	49	3	49
7.52	53	57	4	57
8.03	173	68	12	69
8.54	268	53	19	56
9.04	243	40	17	43
9.55	345	55	25	60
10.06	405	38	28	47
10.56	401	68	28	74
11.07	347	77	24	81
11.57	408	48	29	56
12.08	444	74	31	80
12.58	310	129	22	131
13.09	573	144	40	149

2.3 GEANIE partial gamma-ray measurement

New measurements of ^{239}Pu$(n, 2n\gamma)$ partial cross sections by the GEANIE collaboration (Becker *et al.* [Bec01], Bernstein *et al.* [Ber00], and Younes *et al.* [You00]) have been completed recently. The GEANIE measurement is summarized in Figure 4. ^{239}Pu samples were irradiated with neutrons at the LANSCE/WNR facility and secondary γ-rays characteristic of ^{238}Pu were measured in-beam with an array of Ge detectors (GEANIE). The GEANIE detector array was on the 60° right flight path (60R) at LANSCE/WNR. The LANSCE/WNR facility is a spallation neutron source, and reaction neutron energies were determined via time of flight (flight path $\approx$ 20 m). The incident neutron fluence was measured with fission chambers. Various γ-ray transitions were observed in the GEANIE array [Ber00], the strongest of which was the $6^+ \rightarrow 4^+$ 157 keV transition.

Actinide targets have considerable γ-ray backgrounds from sample radioactivity and target activation. The energy resolution of the γ-ray detectors ($\Delta E/E \sim 0.1\%$) and the energy spectrum of background γ rays determines the feasibility of this type of measurement for a particular γ ray.

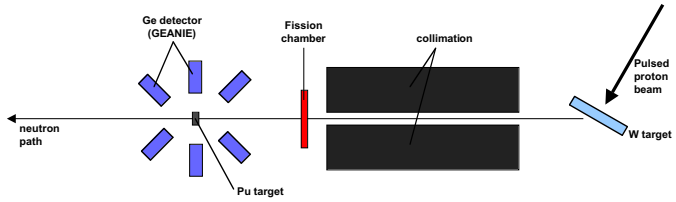

Figure 4: A schematic of the GEANIE collaboration measurement [Bec01].

The reaction cross section for a particular γ-ray transition is given by

$$\sigma_{(n,2n\gamma)} = \frac{N_\gamma}{\varepsilon \Phi \rho_t} \tag{7}$$

where N_γ is the number of γ rays observed, ε is efficiency for detecting these γ rays, ρ_t is the areal number density of the ^{239}Pu target, and Φ is the time-integrated neutron fluence. There are a number of corrections to Equation 7 that are required as discussed in [McN00] including attenuation of the emitted γ rays in the target material and internal conversion.

The neutron fluence was monitored in-beam with one ^{235}U fission chamber and one ^{238}U fission chamber to check for consistency and also because ^{235}U is better at lower E_n. The ENDF/B-VI cross sections and uncertainties were used for this normalization. Systematic uncertainties in Φ, ε and ρ_t and other quantities are adopted from [McN00] and so are only summarized in this paper. Systematic uncertainties in this measurement are estimated at 6%. The statistical uncertainties used in this work are taken from [Ber00] and vary from 3-16% as a function of incident neutron energy. These results are summarized in Section 2.3.1.

The GEANIE measurement has several advantages over the other methods:

- Simultaneous measurement of the partial γ-ray cross sections over the entire incident neutron energy range
- A clear separation of fission and $(n, 2n)$ γ rays; Unambiguous γ-ray lines for several transitions
- No secondary neutron interactions because a thin target (10 mils) was used

However, since the GEANIE detector measured cross sections for specific γ rays that cascade to the ^{238}Pu ground state in $(n, 2n)$ reactions, an appeal must be made to nuclear theory and

modeling to predict the contribution from unmeasured decay branches in order to infer the $(n, 2n)$ cross section. The ratio

$$\frac{\sum\limits_{\gamma\ paths} \sigma^{EXP}_{(n,2n\gamma)}}{\sigma^{EXP}_{(n,2n)}} = \frac{\sum\limits_{\gamma\ paths} \sigma^{MODEL}_{(n,2n\gamma)}}{\sigma^{MODEL}_{(n,2n)}} \tag{8}$$

was found to yield the most consistent results between model calculations, with the least sensitivity to uncertainties in the ^{238}Pu decay level scheme, when deriving $\sigma^{EXP}_{(n,2n)}$ [Bec01].

Nuclear reaction model calculations done with the reaction model codes GNASH [Cha99, Cha01], IDA [Ros99, Che00], and STAPRE [Die00] have recently been completed. The nuclear theory calculations use Hauser-Feshbach compound nucleus theory, together with theories for statistical, direct, pre-equilibrium, and nuclear fission reactions, to model the formation of an initial excited nuclear system following neutron bombardment, and the subsequent decay of the excited nucleus by sequential neutron emission, gamma-ray decay, or fission. Section 2.3.2 discusses the assumptions and uncertainties that are inherent in these model calculations.

2.3.1 Partial cross section results summary

While 8 γ-ray lines in ^{238}Pu were observed in the GEANIE experiment [Ber00], only five of these were used in conjunction with Equation 8 in order to avoid double counting. For example, the ground state band $8^+ \rightarrow 6^+$ transition directly results in an ground state band $6^+ \rightarrow 4^+$ transition. Hence, each transition in the summations of Equation 8 must belong to separate, or non-coincident, decay paths. The ground state band $4^+ \rightarrow 2^+$ transition was not measured due to contamination from a fission γ ray and the $2^+ \rightarrow 0^+$ transition is not observed in the GEANIE experiment because it proceeds almost entirely via internal electron conversion.

As discussed in [McN00], the systematic uncertainty of the γ-ray absorption and internal conversion corrections for particular γ-ray cross sections vary as a function of the target thickness, γ-ray energy, and the electromagnetic character of the transition. In the analysis presented in [Ber00], data taken with 10- and 20-mil targets were summed together, and five transitions were added together. Based on the results of [McN00], an average value of 6% is used as the overall systematic uncertainty of the GEANIE measurement for this evaluation. This systematic uncertainty is considered independent of incident neutron energy. Statistical uncertainties for the numerator of the left side of Equation 8 were taken from Table 9 of [Ber00] for the 157-keV $6^+ \rightarrow 4^+$ transition and then reduced by a factor of 1.45 to account for the additional statistics in the other four γ rays included in the summation. The statistical uncertainties ranged from 3-16% as a function of incident neutron energy. The statistical and systematic uncertainties used in this evaluation are summarized below in Table 7.

2.3.2 Reaction model results summary

Several different reaction model calculations have been performed to provide the input for the right-hand side of Equation 8 in order to infer the ^{239}Pu$(n, 2n)$ cross section from the GEANIE partial γ-ray cross sections. Calculations with GNASH [Cha99] and IDA [Ros99, Che00] have

been finalized and documented, including some sensitivity studies. Preliminary calculations with STAPRE [Die00] have also been done, but these are not yet documented. The STAPRE results support the conclusions from both GNASH and IDA results. The results for GNASH and IDA are summarized in Figure 5.

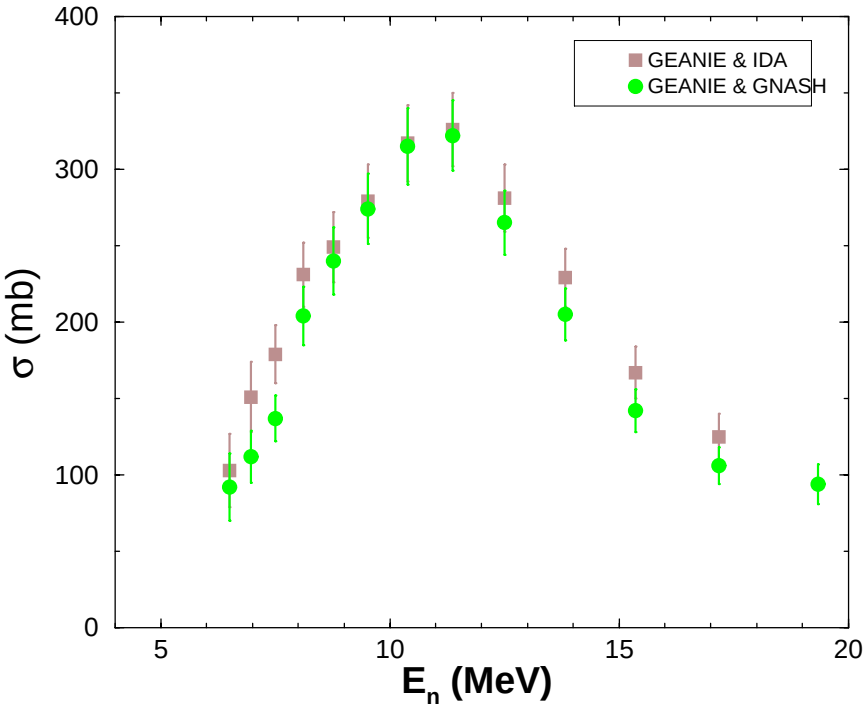

Figure 5: Comparison of inferred ^{239}Pu$(n, 2n)$ cross section using Equation 8 with two separate Hauser-Feshbach reaction model codes: GNASH and IDA. Uncertainties shown are the experiment only.

An important point to make regarding these model calculations is that since Equation 8 requires a ratio of partial cross sections to the total $(n, 2n)$ cross section, factors which only affect the scale or magnitude of the $(n, 2n)$ cross section do not affect the partial-to-total ratios — in particular the magnitude of the reaction cross section. Factors which do affect the ratio can be broken down into two main parts: (1) processes which affect the initial entry distribution of ^{238}Pu residual nuclei in (E, J^{π}) space (2) processes which affect the ensuing (mostly) γ-ray cascade to the ^{238}Pu ground state.

Aspects of the models which affect the initial entry distribution include

- Coupled-channel optical model; transmission coefficients (partial waves)
- Exciton pre-equilibrium particle emission model
- Bjornholm-Lynn double-humped fission model

The optical model has been well benchmarked in terms of its ability to reproduce particle angular distributions, and so it is reasonable to assume that the spin transfer in absorption and

emission is well-characterized by this model and that sensitivity studies provide a good estimate of the uncertainties. The pre-equilibrium emission and fission models are more problematic. In the case of pre-equilibrium emission, the GNASH calculations assume that the spin transfered to the residual nucleus was given by the compound evaporation model using the optical model to calculate transmission coefficients. This is clearly incorrect, and so the assumption will have some adverse systematic affect on the ratio results, particularly for $E_n > 12$ MeV where pre-equilibrium neutron emission begins to dominate for the first neutron emitted. A full treatment of this process is likely to result in an increase in the inferred $(n, 2n)$ cross section above 12 MeV.[4] The Bjornholm-Lynn fission model results in a partial-wave dependence of fission, due to changes in the level density and barrier heights. This model is phenomenological and has not been benchmarked in its ability to reproduce the partial-wave distributions accurately.

The γ-ray cascade models used for these calculations contain very little nuclear structure information and rely mostly on the statistical decay model coupled with Giant Dipole Resonance strength functions. The statistical model for γ-ray decay is well benchmarked, particularly for $E_x - E_{yrast} \gtrsim 4 - 5$ MeV. At lower excitation energies, nuclear structure effects start to play a significant role. By using Equation 8, one is effectively asking the model to account for the amount of statistical decay which bypasses the γ-ray transitions included in the summation. It is possible, however, that there are some unobserved decay paths that are not well represented by the statistical model. In this sense, the GEANIE results represent a lower limit to the $(n, 2n)$ cross section.

For this evaluation, the model results from GNASH [Cha01] were used to infer the GEANIE cross section. There were two reasons for this: (1) GNASH is better documented than IDA and the results more easily reproduced and (2) GNASH and STAPRE benchmark calculations are in good agreement while the IDA benchmarks had discrepancies that are not fully understood.

Parameter sensitivity studies were carried out with the GNASH code [Cha01]. Reaction model parameters were varied within one-sigma limits and the results were interpreted as an uncertainty in the calculated partial-to-total ratios. These results are shown in Figure 6. The evaluated uncertainties in the model calculations of the partial-to-total ratio were determined by using the results shown in both Figures 5 and 6, and the values used are tabulated in Table 7.

[4]Preliminary calculations predict that pre-equilibrium emission is more likely to leave the residual nucleus in a low-spin state ($\ell \approx 4\hbar$) than compared with a pure compound nucleus model. This lower spin tends to result in a smaller calculated partial-to-total ratio. A smaller calculated partial-to-total ratio results in a larger inferred $(n, 2n)$ cross section per Equation 8.

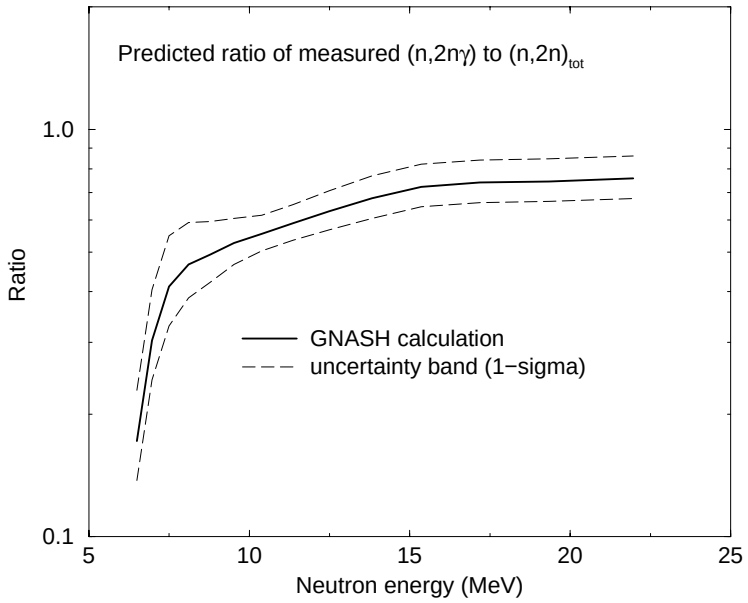

Figure 6: The sum of the observed partial γ-ray cross section divided by the total ^{239}Pu$(n, 2n)$ cross section as calculated by GNASH [Cha01] (—). A one-sigma uncertainty band based on sensitivity studies is also shown (- - -). These calculations were used to infer the total $(n, 2n)$ cross section from the GEANIE data.

2.3.3 Summary of evaluated results and uncertainties

The GEANIE ^{239}Pu $\sigma_{(n,2n)}$ data values and relative uncertainties used in this evaluation are given in Table 7. The statistical and systematic uncertainties in the measurement are given, as well as uncertainties assumed for the model calculations.

Table 7: The GEANIE ^{239}Pu $\sigma_{(n,2n)}$ data values and relative uncertainties used in this evaluation.

		Relative uncertainties			
E_n (MeV)	$\sigma_{(n,2n)}$ (mb)	Statistical	Systematic	Model	Combined
6.5	92	0.16	0.06	0.25	0.30
6.97	112	0.10	0.06	0.25	0.28
7.5	137	0.06	0.06	0.25	0.26
8.11	204	0.05	0.06	0.21	0.23
8.77	240	0.05	0.06	0.17	0.19
9.52	274	0.04	0.06	0.13	0.15
10.39	315	0.03	0.06	0.10	0.12
11.37	322	0.03	0.06	0.10	0.12
12.5	265	0.03	0.06	0.11	0.13
13.82	205	0.04	0.06	0.12	0.14
15.36	142	0.06	0.06	0.12	0.15
17.18	106	0.07	0.06	0.12	0.15
19.34	94	0.08	0.06	0.12	0.16
21.96	105	0.07	0.06	0.12	0.15

3 Consistency with other experimental data

A straightforward covariance analysis of available experimental data on the ^{239}Pu$(n,2n)$ cross section is very limiting. An approach is needed in order to

- Rectify inconsistent measurements
- Include other nuclear data relevant to the ^{239}Pu$(n,2n)$ cross section into the evaluation in a consistent manner

In this Section, careful attention is paid to the impact of other nuclear data on the expected shape and magnitude of the ^{239}Pu$(n,2n)$ cross section as a function of E_n. Features of the shape of the $\sigma_{(n,2n)}$ based on general nuclear physics arguments and measurements on other actinide nuclei are discussed in Section 3.1. Nuclear data and supporting arguments are used to derive a 15% number for the ^{239}Pu$(n,2n)$ cross section at $E_n \approx 11$ MeV in Section 3.2.

3.1 Shape of the $(n,2n)$ cross section

The first place to look for information on the ^{239}Pu$(n,2n)$ cross section is measurements on other actinide nuclei. Figure 7 summarizes the $(n,2n)$ cross section measurements in ^{238}U and ^{232}Th, two nuclei that have been particularly well studied because conditions are favorable for activation measurements. These measurements confirm that the general features of the shape of the $(n,2n)$ cross section as a function of the incident neutron energy is well understood in the context of the compound nucleus and pre-equilibrium reaction models. In the compound nucleus model, the $(n,2n)$ reaction cross section increases rapidly from threshold until competition from the (n,n') channel is negligible. In a simple evaporation model that is adequate to describe this behavior, the ratio of the compound $(n,2n)$ cross section to the entire compound nuclear cross section (neglecting fission) is given by

$$\frac{\sigma_{(n,2n)}}{\sigma_{(n,2n)}+\sigma_{(n,n')}} = \frac{\int_{E_{thr}}^{E_n} (E_n - E_x)^{\frac{1}{2}} \rho(E_x)\, dE_x}{\int_{0}^{E_n} (E_n - E_x)^{\frac{1}{2}} \rho(E_x)\, dE_x} \tag{9}$$

where E_n is the incident neutron energy, E_{thr} is the threshold energy for the ^{239}Pu$(n,2n)$ reaction, and $\rho(E_x)$ is the nuclear level density for ^{239}Pu at excitation energy E_x. The behavior exhibited by Equation 9 is shown in Figure 8 for ^{239}Pu using a constant temperature model for the nuclear level density, $\rho(E_x) = e^{E_x/0.457}$ (E_x in MeV). By about $E_n = E_{thr} + 3$ MeV, the compound (n,n') channel is negligible and the $(n,2n)$ cross section is in a plateau region. When the $(n,3n)$ channel opens up energetically, essentially the reverse happens, and the $(n,2n)$ channel decreases rapidly until only events involving pre-compound neutron emission populate the $(n,2n)$ channel. The expected behavior at threshold is inconsistent with the Frehaut *et al.* data set (and completely inconsistent with the Mather *et al.* data). As a result, the evaluation has relied on the GEANIE data set in this energy region. This is discussed more fully in Section 4.

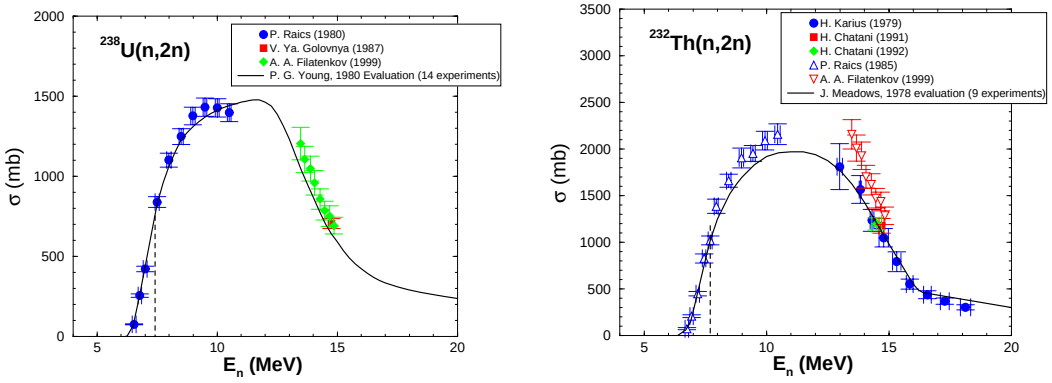

(a) ^{238}U (b) ^{232}Th

Figure 7: A summary of available $(n, 2n)$ cross section data on two actinide nuclei that have been particularly well measured: ^{238}U (a) and ^{232}Th (b).

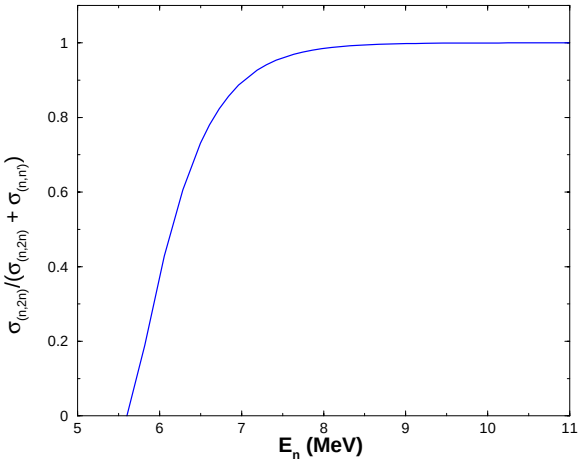

Figure 8: The ratio of $\sigma_{(n,2n)}$ to $\sigma_{(n,2n)} + \sigma_{(n,n')}$ for n+^{239}Pu using Equation 9 with $\rho(E_x) = e^{E_x/0.457}$ (E_x in MeV).

3.2 Magnitude of the $(n, 2n)$ cross section

General theoretical considerations provide a framework for rectifying inconsistent measurements. They also allow high-quality nuclear data (separate from direct measurements of an $(n, 2n)$ cross sections) to be used to independently determine $\sigma_{(n,2n)}$ using simple relations, *e.g.* $\sigma_{(n,2n)} = \sigma_{non} - \sigma_{(n,f)} - \sigma_{(n,n')}$ where σ_{non}, $\sigma_{(n,f)}$, and $\sigma_{(n,n')}$ are measured quantities discussed below. The concept of using other measurements to derive $\sigma_{(n,2n)}$ was first discussed by Vonach *et al.* [Von90] for non-fissionable isotopes at 14 MeV. This approach, as applied to the ^{239}Pu$(n, 2n)$, has been discussed thoroughly by Anderson *et al.* [And00] and Navratil *et al.* [Nav00]. In the present evaluation, the focus has been on applying this concept in a rigorous, data-driven approach.

The simplest statement one can make regarding neutron-induced reaction cross sections is that the total cross section, σ_T, is the sum of all its parts. Because of the large Coulomb barrier in actinide nuclei, charged-particle exit channels can be ignored (reaction cross sections $\lesssim 10$ mb). Hence, below the $(n, 3n)$ threshold

$$\sigma_T = \sigma_e + \sigma_{D.I.} + \sigma_{(n,f)} + \sigma_{(n,n')} + \sigma_{(n,2n)} \tag{10}$$

where σ_e is elastic scattering and $\sigma_{D.I.}$ is direct inelastic scattering. The non-elastic cross section, σ_{non}, is defined as

$$\sigma_{non} = \sigma_T - \sigma_e - \sigma_{D.I.} \tag{11}$$

because this quantity can be directly measured by means of the sphere-transmission technique [Mac57]. The direct inelastic cross section has been lumped together with the elastic cross section because experimental resolutions are often not able to distinguish neutrons losing a small ($\lesssim 120$ keV) amount of energy from elastically scattered neutrons on actinide targets.

From Eqs. 10 and 11 one can derive the following equation for the $(n, 2n)$ cross section:

$$\sigma_{(n,2n)} = \sigma_{non} - \sigma_{(n,f)} - \sigma_{(n,n')} \tag{12}$$

Because measurements of neutron reactions on ^{238}U, ^{235}U and ^{232}Th targets are better characterized than those for ^{239}Pu, it is natural to use these more precise measurements coupled with scaling laws in place of less precise or non-existent measurements on ^{239}Pu in order to determine $\sigma^{^{239}Pu}_{(n,2n)}$. These four actinide nuclei can be simply related to each other using theoretical constraints that have been well-benchmarked by experiment. Internal consistency is obtained by requiring Equation 12 to be satisfied for all four nuclei (^{239}Pu, ^{238}U, ^{235}U and ^{232}Th) while simultaneously applying two theoretical constraints discussed below.

The (n, f) and $(n, 2n)$ cross sections of these nuclei are quite well known (except for ^{239}Pu$(n, 2n)$). For example, $\sigma^{^{238}U}_{(n,2n)}$ is extensively measured and is known to $\approx 5\%$ for $E_n \approx 11$ MeV. The experimentally-determined cross section values used in this evaluation are listed in Table 8. Both σ_{non} and $\sigma_{(n,n')}$ are less accurately known and measured at fewer energies than $\sigma_{(n,f)}$. However, some simple reaction theory arguments, well supported by measurements, can be used to constrain σ_{non} and $\sigma_{(n,n')}$ values between nuclei. The constraint for $\sigma_{(n,n')}$ is the

most limiting, as it is only applicable in the plateau region of $\sigma_{(n,2n)}$ for $E_n \gtrsim 10 - 11$ MeV. Since the $^{238}\mathrm{U}(n,3n)$ channel opens up at about $E_n = 11.3$ MeV, Equation 12 can only effectively be used with the σ_{non} and $\sigma_{(n,n')}$ constraints for $E_n \approx 11$ MeV. These constraints are fully described below in Sections 3.2.1 and 3.2.2.

Table 8: A summary of various experimental cross sections used as input in this evaluation at $E_n = 11$ MeV for ^{239}Pu, ^{238}U, ^{235}U, and ^{232}Th. The $\sigma_{(n,f)}$ and $\sigma_{(n,2n)}$values were taken from recent evaluations in ENDL [ENDL] and ENDF/B-VI [ENDF]. The values used for $\sigma_{(non)}$ and $\sigma_{(n,n')}$ are discussed in the text.

	$\sigma_{(n,2n)}$ (mb)	$\sigma_{(non)}$ (mb)	$\sigma_{(n,f)}$ (mb)	$\sigma_{(n,n')}$ (mb)
^{239}Pu	??	2900(100)	2234(28)	constrained
^{235}U	800(100)	constrained	1726(19)	constrained
^{238}U	1462(73)	constrained	983(13)	345(55)
^{232}Th	2150(150)	constrained	305(6)	constrained

Equation 12 combined with the information summarized in Table 8 (including the σ_{non} and $\sigma_{(n,n')}$ constraints) defines a system of equations which can be solved to derive the $^{239}\mathrm{Pu}(n,2n)$ cross section for $E_n = 11$ MeV. The details of this procedure are fully discussed in Reference [Nav00]. The [Nav00] results are summarized here by reproducing Tables III and IV from [Nav00], who find:

$$\sigma^{239\mathrm{Pu}}_{(n,2n)}(E_n = 11 \text{ MeV}) = 323(45) \text{ mb} \tag{13}$$

Table 9: Reproduction of TABLE III of [Nav00]. The values and ranges, in millibarns, of the various cross sections used to derive $^{239}\mathrm{Pu}(n,2n)$ at $E_n = 11$ MeV.

	$\sigma_{(non)}$ (mb)	$\sigma_{(n,f)}$ (mb)	$\sigma_{(n,n')}$ (mb)	$\sigma_{(n,2n)}$ (mb)
^{239}Pu		2234	290-400	100-700
^{235}U		1726	$\sigma^{239}_{(n,n')} \pm 20$	700-900
^{238}U	2700-3100	983	$\sigma^{239}_{(n,n')} \pm 20$	1414-1594
^{232}Th		305	$\sigma^{239}_{(n,n')} \pm 20$	2000-2300

Table 10: Reproduction of TABLE IV of [Nav00]. The average values and standard deviations, in millibarns, of the various cross sections determined from solving the system of equations given by Equation 12 for each nucleus at $E_n = 11$ MeV.

	$\sigma_{(non)}$ (mb)	$\sigma_{(n,n')}$ (mb)	$\sigma_{(n,2n)}$ (mb)
^{239}Pu	2904(64)	347(36)	323(45)
^{235}U	2872(63)	347(39)	799(40)
^{238}U	2896(64)	359(38)	1554(38)
^{232}Th	2847(63)	352(39)	2190(43)

3.2.1 σ_{non} constraint

Non-elastic cross section measurements can be well described in the relevant energy region by the black nucleus approximation (see, for example, [Gri75])

$$\sigma_{non} = \pi(R + \lambda\!\!\!^{-})^2 \tag{14}$$

where R is the radius of the target nucleus and $\lambda\!\!\!^{-}$ is the reduced neutron wavelength, $\hbar/\sqrt{2m_nE_n}$.

There is extensive experimental evidence that the change in σ_{non} over such a small mass range is (1) small ($\approx 2\%$), (2) accurately predicted by nuclear optical models, and (3) not sensitive to shell-model effects for incident neutron energies above 5 MeV. For example, differential elastic scattering cross sections have been precisely measured for ^{208}Pb and ^{209}Bi under the same experimental conditions [Ann85] and the measured cross section difference of 2.0(1.0)% for $E_n = 7$ MeV was well reproduced by nuclear optical model calculations. Also, Dietrich *et al.* [Die00] have precisely measured the neutron total cross section difference ($\sigma_T^{^{238}U} - \sigma_T^{^{232}Th}$) and have concluded that this difference is predicted by the nuclear optical model within 0.3% or 20 mb.

Therefore, Eq. 14 was used as an overall constraint and also as a way to combine measurements. The σ_{non} data published by MacGregor *et al.* [Mac63] is used in this evaluation, as this was judged to be the most reliable set of non-elastic neutron cross section measurements available for actinides near $E_n = 11$ MeV. Based on MacGregor *et al.* measurements on ^{235}U, ^{238}U, and ^{239}Pu at $E_n = 11.9$ and 14.1 MeV, we determined that $\sigma_{non} = 2.90(10)$ barns at $E_n = 11$ MeV in ^{239}Pu. This experimentally determined value was used as input in [Nav00] and was allowed to vary over two sigma as indicated in Table 9. The mean values of σ_{non} determined by the [Nav00] variation procedure are summarized in Table 10. The mean value for ^{239}Pu, $\sigma_{non} = 2904(64)$ mb, is consistent with the 2900(100) mb value derived from MacGregor *et al.* The uncertainty of the [Nav00] value is smaller because of the other nuclear data that was incorporated into the variation procedure by using Equation 12.

3.2.2 $\sigma_{(n,n')}$ constraint

The quantity $\sigma_{(n,n')}$ is more easily understood if broken down into pre-equilibrium and compound components. As discussed above in Section 3.1, the compound component is negligible in the plateau region. Hence, in the plateau region, $\sigma_{(n,n')}$ is nearly entirely due to pre-equilibrium neutron emission. Pre-equilibrium neutron cross sections have been measured for the n+^{238}U by both Kammerdiener [Kam72] and Baba *et al.* [Bab89], but n+^{239}Pu has only been measured by Kammerdiener. Other experimental work (for example, [Gri98]) and semi-classical pre-equilibrium models [Bla83] indicate that the shape and magnitude of pre-equilibrium neutron emission is essentially unchanged from $A = 232 - 239$, except for overall energy shifts due to odd-even pairing effects. The Kammerdiener [Kam72] measurements limit the difference between pre-equilibrium neutron emission yields of ^{238}U and ^{239}Pu to about 20 mb. The n+^{238}U Baba *et al.* data has significantly better energy resolution and so was used for this evaluation in order to derive $\sigma_{(n,n')}$ at 11 MeV in all four actinide nuclei.

Figure 9 summarizes the Baba [Bab89] data. In order to derive $\sigma_{(n,n')}$, the data shown in Figure 9 (with fission neutrons subtracted) have been integrated from the $(n, 2n)$ threshold to $E_n - 1.6$ MeV, where 1.6 MeV was estimated to be the energy gap in the nuclear level density. These high-energy neutron emission events must belong to the (n, n') channel since the residual nucleus has too little energy to emit another neutron. It is also assumed, apart from direct collective excitations already accounted for in Equation 11, that the pre-equilibrium mechanism is the only way to populate the (n, n') channel at these incident neutron energies, *i.e.* compound nuclear processes are negligible as discussed in Section 3.1. In this way, the ^{238}U(n, n') cross section at $E_n = 14$ MeV was estimated to be 300(47) mb. Based on the time it takes for the incident neutron to traverse the nucleus, it is expected that the pre-equilibrium neutron emission cross section should vary as $E_n^{-1/2}$. This trend is consistent with the GEANIE data for $(n, n'\gamma)$ lines. As a result, the ^{238}U(n, n') cross section at $E_n = 11$ MeV has been set to $\sqrt{14/11} \times 300(47) = 345(55)$ mb. Because [Gri98] and [Kam72] support suggest that this value is insensitive to atomic number, the (n, n') cross sections on ^{232}Th, ^{235}U, and ^{239}Pu have been constrained to be within 20 mb of the ^{238}U value.

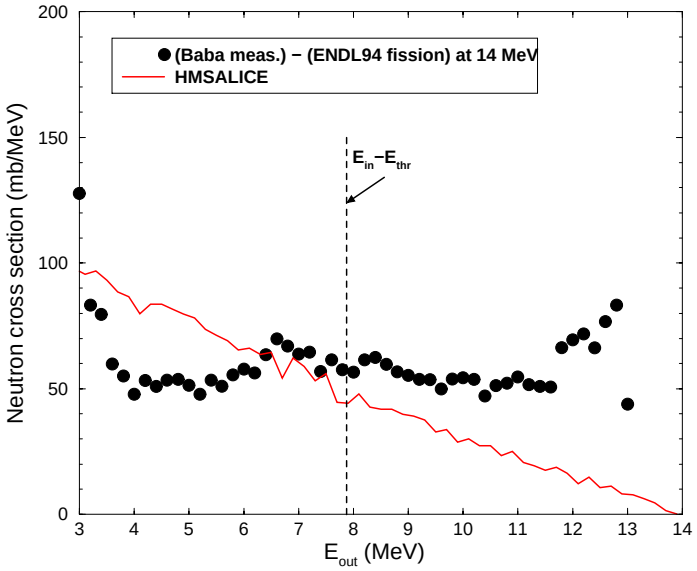

Figure 9: The Baba data [Bab89] in ^{238}U (•) after the elastic peak and ENDF/B-VI fission neutron spectrum have been subtracted. This pre-equilibrium neutron emission spectrum for $E_n = 14$ MeV is compared with a Monte Carlo exciton model calculation (—) using HMSALICE [Bla83]. It should be noted that the HMSALICE calculation includes events with pre-equilibrium neutron emission before fission, whereas the data (fission neutrons subtracted) do not.

4 Recommended ^{239}Pu$(n, 2n)$ cross section and uncertainties

The data values and uncertainties used in this evaluation are plotted in Figure 10 and are compared to general expectations of the shape and magnitude of the ^{239}Pu$(n, 2n)$ cross section as discussed in Section 3. The black lines denoting the rise and fall of the $(n, 2n)$ cross section at the $(n, 2n)$ and $(n, 3n)$ threshold are intended to guide the eye, not to communicate accurate information. However, the Navratil and McNabb [Nav00] data point at $E_n = 11$ MeV is solidly based on nuclear data, and is a measure of the ^{239}Pu$(n, 2n)$ cross section independent of the other direct measurements discussed.

]

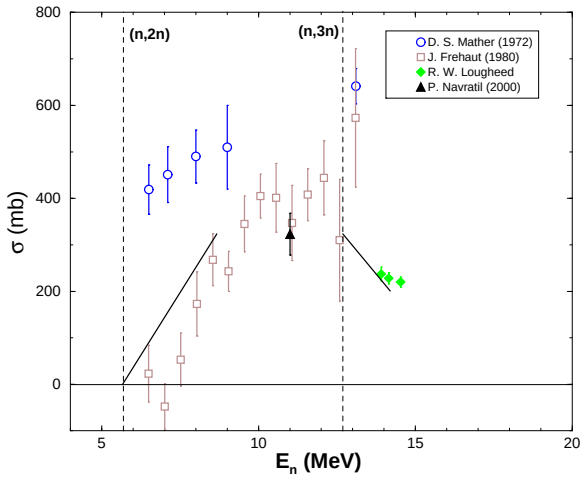

Figure 10: The ^{239}Pu$(n, 2n)$ data circa 1985 used in this evaluation is compared to general expectations of the shape and magnitude of the $(n, 2n)$ cross section based on other nuclear data.

It is clear from Figure 10 that the Mather *et al.* data is inconsistent with both nuclear physics expectations and the other data sets. In Section 2.2 it was noted that Mather *et al.* apparently did not have the capability to account for down-scattered neutrons incident on the target, a major issue. The magnitude of this effect can be judged by comparing the Mather *et al.* data with Frehaut *et al.* *et al.* For these reasons, we have rejected the Mather *et al.* data set.

The Frehaut *et al.* data is systematically too low near threshold. As discussed in Section 2.2, there are sizeable systematic uncertainties in the neutron counting technique as applied to ^{239}Pu$(n, 2n)$. These uncertainties arise from systematic corrections which vary as a function of incident neutron energy. The Frehaut *et al.* data is clearly too low near threshold and the uncertainties are very large at the highest neutron energies. For these reasons, the Frehaut *et al.* data set has not been included when combining data sets for this evaluation.

The Lougheed *et al.* data is consistent with our expectations based on other nuclear data, as can be seen from Figure 10. In addition, as discussed in Section 2.1, it is the most precise

measurement of the $(n, 2n)$ cross section, with the uncertainty estimated at $\pm 6\%$.

Our conclusion is that the GEANIE data coupled with Hauser-Feshbach modeling, the Lougheed *et al.* irradiation measurement, and the data point at $E_n = 11$ MeV derived from other nuclear data in Section 3 are the most reliable data sets for determining the shape and magnitude of the ^{239}Pu$(n, 2n)$ cross section. Figure 11 summarizes the data and the evaluation. The uncertainties on all data points reflect the statistical and systematic uncertainties used in this evaluation. The uncertainties on the GEANIE data points also include the uncertainties ascribed here to the reaction modeling as shown in Figure 6. The evaluation follows the GEANIE data at threshold into the peak region. The cross section in the 14 MeV region is given by a weighted average of the GEANIE and Lougheed *et al.* results. One possible explanation as to why the Lougheed *et al.* data are larger than the GEANIE data is that the spin transfer in the pre-equilibrium models used to infer the GEANIE cross section are inadequate as discussed in Section 2.3.2. Another possibility is that unobserved states (possibly isomeric) are populated in the GEANIE measurement but are not accounted for with the statistical γ-ray decay model.

A one-sigma uncertainty estimate based on a covariance matrix analysis is also given in Figure 11. This evaluation is consistent with the Frehaut *et al.* data within an uncorrelated one-sigma uncertainty, but the shape is significantly different. Table 11 contains a tabulation of the evaluation results including one-sigma uncertainties.

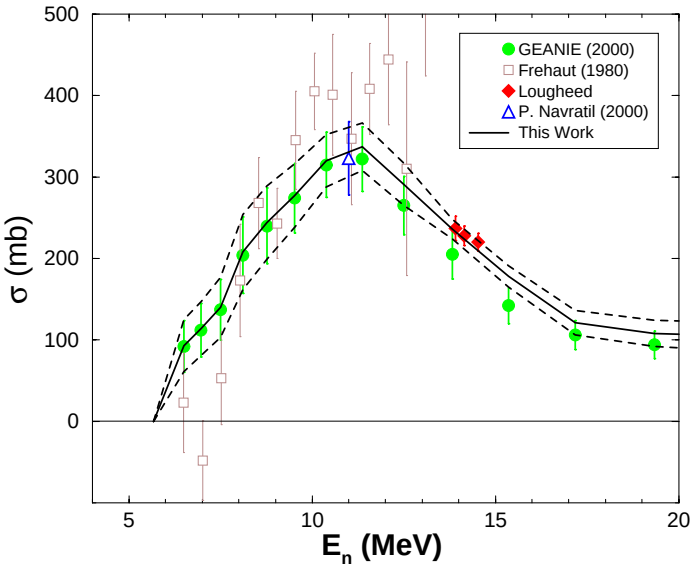

Figure 11: The evaluation of ^{239}Pu$(n, 2n)$ cross section and one-sigma uncertainty limits are compared with the data used in this evaluation.

Table 11: The evaluated ^{239}Pu$(n, 2n)$ cross section.

E_n (MeV)	$\sigma_{(n,2n)}$ (mb)	Relative uncertainty
5.67	0	—
6.5	93	0.34
6.97	114	0.29
7.5	140	0.26
8.11	208	0.22
8.77	244	0.18
9.52	277	0.14
10.39	320	0.10
11.37	337	0.09
12.5	291	0.09
13.82	236	0.05
15.36	178	0.07
17.18	121	0.12
19.34	108	0.15
21.96	104	0.17

This evaluation is compared to previous evaluations in Figures 12 (LLNL) and 13 (LANL). The 1984 evaluation by Blann [Bla84] was based on calculation: a Weisskopf-Ewing reaction model with a pre-equilibrium model and experimentally-based fission probabilities. Optical model parameters and fission probabilities were varied within reasonable ranges and an average result was quoted for the evaluation. Blann recommended an uncertainty on the order of 10% for E_n from 9 to 15 MeV, with larger uncertainties near threshold. The agreement with the present evaluation is excellent. The ENDL92 evaluation [ENDL] was based on the Frehaut *et al.* and Lougheed *et al.* data sets. The difference between ENDL92 and this evaluation below 12 MeV is that this evaluation is largely based on the new GEANIE results rather than the Frehaut *et al.* data. The ENDL92 evaluation is too high at medium neutron energies and too low near threshold.

In Figure 13 this evaluation is compared to two previous ENDF/B (LANL) evaluations [You91]. Both of these evaluations were taken from Hauser-Feshbach reaction models with a pre-equilibrium model and fission barrier parameters determined from fits to available data. The difference between these two calculations may result from different optical model parameters used to calculate the reaction cross section and different fission barrier parameters. The current evaluation is in substantial disagreement with both of these previous evaluations, except near $E_n = 14$ MeV.

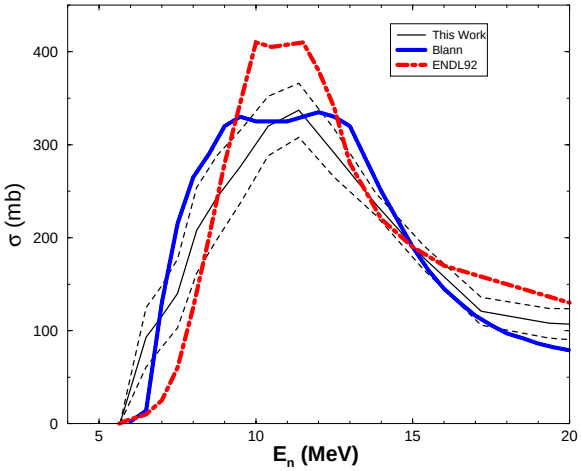

Figure 12: The current evaluation compared to previous evaluations done at LLNL [Bla84, ENDL].

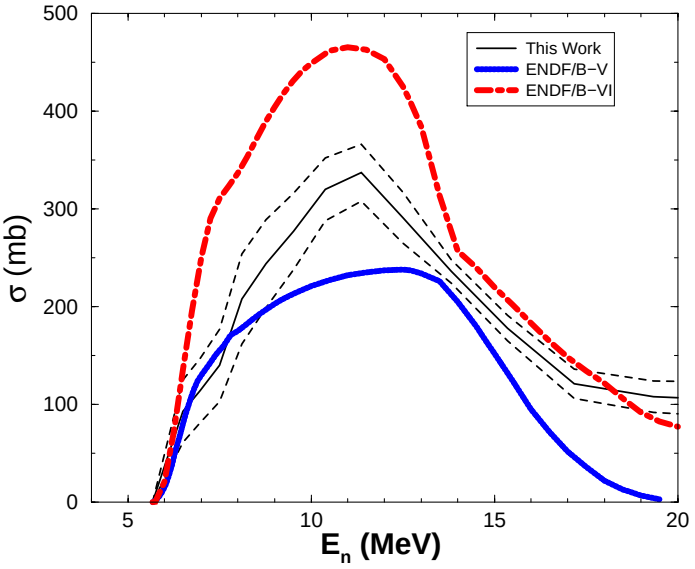

Figure 13: The current evaluation compared with previous ENDF/B evaluations [You91].

In summary, an evaluation of the ^{239}Pu$(n, 2n)$ cross section based on experimental data has been presented including a detailed evaluation of uncertainties. The results have been tabulated in Table 11. This evaluation was prompted by new measurements of ^{239}Pu$(n, 2n\gamma)$ partial cross sections by the GEANIE collaboration (Becker *et al.* [Bec01]. These new data, coupled with reaction model calculations, have been incorporated into this evaluation. This new evaluation has taken into consideration the following information:

- Partial γ-ray cross section measurements by GEANIE (Becker *et al.* [Bec01], Bernstein *et al.* [Ber00], Younes *et al.* [You00], and McNabb *et al.* [McN00]); These measurements cover the energy range from threshold to 20 MeV.
- Nuclear reaction model calculations with GNASH, IDA, and STAPRE (Chadwick and Young [Cha99, Cha01], Chen *et al.* [Che00], and Dietrich *et al.* [Die00])
- 14-MeV activation measurements by Lougheed *et al.* [Lou00]
- Neutron counting measurements by Frehaut *et al.* [Fre85] and Mather *et al.* [Mat72]; These measurements cover the energy range from threshold to 15 MeV.
- Other nuclear data on ^{239}Pu and other actinide nuclei, including total, reaction, elastic, inelastic, fission, and $(n, 2n)$ measurements [Nav00, McN00]

5 Acknowledgements

The authors would like to thank Ron Lougheed, Hong Chen, and Erich Ormand for providing results prior to publication. This work was performed under the auspices of the U. S. Department of Energy by the Lawrence Livermore National Laboratory under contract W-7405-ENG-48 and by the Los Alamos National Laboratory under contract W-4705-ENG-36.

References

[And00] J. D. Anderson, R. W. Bauer, J. A. Becker, F. S. Dietrich, and D. P. McNabb, "An Alternate Approach to the ^{239}Pu$(n, 2n)$ Cross Section," UCRL-ID in preparation (2000).

[Ann85] J. R. M. Annand and R. W. Finlay, "A low-energy optical-model analysis of ^{208}Pb and ^{209}Bi," Nucl. Phys. **A443**, 249 (1985).

[ASTM] American Society for Testing and Materials, Method E 496 (1996).

[Bab89] M. Baba, "Measurements of Prompt Fission Neutron Spectra and Double Differential Neutron Inelastic Scattering Cross Sections for ^{238}U and ^{232}Th," Report JAERI-M-89-143 (1989).

[Bec01] J. A. Becker *et al.*, "???," UCRL-ID in preparation (2001).

[Ber00] L. A. Bernstein *et al.*, "Measurement of several ^{239}Pu(n,xn) partial γ-ray cross sections for $x \leq 3$ using GEANIE at LANSCE/WNR," UCRL-ID-140308 (2000); L. A. Bernstein *et al.*, "A New Method for Extracting Channel Cross Sections from γ-rays: The ^{239}Pu$(n, 2n\gamma)$ Cross Section," manuscript in preparation for Phys. Rev. C (2001).

[Bla83] M. Blann and H. K. Vonach, Phys. Rev. **28**, 1475 (1983); see also M. Blann, "Recent Progress and Current Status of Preequilibrium Reaction Theories and Computer Code Alice," in *Workshop on Computation and Analysis of Nuclear Data Relevant to Nuclear Energy and Safety*, M. K. Mehta and J. J. Schmidt eds., World Scientific, p. 517-578 (1993).

[Bla84] M. Blann and R. M. White, "Nuclear Modeling of the ^{239}Pu(n, xn) Excitation Function," UCID-19980 (1984).

[Car93] A. D. Carlson *et al.*, "The ENDF/B-VI Neutron Cross Section Measurement Standards," Document ENDF-351 available from the National Nuclear Data Center or Document NISTIR-5177 available from NIST, May 1993.

[Cha99] M. B. Chadwick and P. G. Young, "Calculated plutonium reactions for determining ^{239}Pu$(n, 2n)^{238}$Pu," LAUR-99-2885 (1999);

[Cha01] M. B. Chadwick and P. G. Young, "Calculated plutonium reactions for determining ^{239}Pu$(n, 2n)^{238}$Pu: Summary of final results," LAUR in preparation (2001).

[Che00] H. Chen *et al.*, "The ^{239}Pu$(n, 2n)^{238}$Pu Cross Section Inferred from IDA Calculations and GEANIE Measurements," UCRL-ID submitted (2000).

[Die00] F. S. Dietrich, private communication (2000).

[ENDF] ENDF data base available at http://www.nndc.bnl.gov/.

[ENDL] ENDL data base available at http://www-ndg.llnl.gov/llnl/nds.cgi/lib/endl.

[Fil99] A. A. Filatenkov *et al.*, EXFOR data base entry 41240 at http://www.nndc.bnl.gov/nndc/exfor/.

[Fre80] J. Frehaut, A. Bertin, and R. Bois, "Measurement of the ^{235}U$(n, 2n)$ Cross Section Between Threshold and 13 MeV," Nucl. Sci. Eng. **74**, 29 (1980), and references therein.

[Fre85] J. Frehaut *et al.*, "(n,2n) Cross Sections of ^{2}H and ^{239}Pu," Radiation Effects **96** 219 (1986); see also J. Frehaut, A. Bertin, and R. Bois, EXFOR data base entry 21971 at http://www.nndc.bnl.gov/nndc/exfor/.

[Fu82] C. Y. Fu and D. M. Hetrick, "Experience in Using the Covariances of Sone ENDF/B-V Dosimetry Cross Sections: Proposed Improvements and Additions of Cross-reaction Covariances," Proc. Fourth ASTM-Euratom Symp. on Reactor Dosimetry, Gaithersburg, Maryland, March 22-26, US National Bureau of Standards, 877 (1982).

[Gar92] I. Garlea *et al.*, EXFOR data base entry 31459 at http://www.nndc.bnl.gov/nndc/exfor/.

[Gri75] S. M. Grimes, J. D. Anderson, and C. Wong, "Odd-Even Effects in Pre-Equilibrium Processes," UCRL-77438 (1975).

[Gri98] S. M. Grimes *et al.*, "Justification of a Simple Ramsauer Model for Neutron Total Cross Sections," Nucl. Sci. Eng. **130**, 340 (1998).

[Hel98] R. G. Helmer, private communication (1998). The quoted values were taken from the DDEP and IAEA-TECDOC-619 evaluations.

[Ike88] Y. Ikeda *et al.*, EXFOR data base entry 22089 at http://www.nndc.bnl.gov/nndc/exfor/.

[Kam72] J. L. Kammerdiener, "Neutron Spectra Emitted by ^{239}Pu, ^{238}U, ^{235}U, Pb, Nb, Ni, Al, and C Irradiated by 14 MeV Neutrons," UCRL-51232 (1972).

[Kob88] K. Kobayashi and I. Kimura, EXFOR data base entry 22093 at http://www.nndc.bnl.gov/nndc/exfor/.

[Lou00] R. W. Lougheed, private communication (2000).

[Mac57] M. H. MacGregor, W. P. Ball, and R. Booth, "Nonelastic Neutron Cross Sections at 14 MeV," Phys. Rev. **108**, 726 (1957).

[Mac63] M. H. MacGregor, W. P. Ball, and R. Booth, "Nonelastic Neutron Cross-Sections Measurements on Li^{6}, Li^{7}, U^{235}, U^{238}, Pu^{239}, at 8.1, 11.9, and 14.1 MeV," Phys. Rev. **130**, 1471 (1963).

[Mat72] D. S. Mather *et al.*, "Measurement of (n,2n) Cross Sections for Incident Energies between 6 and 14 MeV," AWRE Report No. 072/72 (1972).

[McN00] D. P. McNabb *et al.*, "Uncertainty budget and efficiency analysis for the ^{239}Pu(n,2$n\gamma$) partial reaction cross-section measurements," UCRL-ID-139906 (2000).

[Nav00] P. Navratil and D. P. McNabb, "Calculation of the ^{239}Pu$(n, 2n)$ cross section by the subtraction and ratio methods," UCRL-ID-140697 (2000).

[Ros99] M. A. Ross, H. Chen, G. Reffo, and R. M. White, "The ^{239}Pu$(n, 2n)^{238}$Pu Cross Section: Preliminary Calculations," UCRL-ID-133497 (1999).

[Ryv89] T. B. Ryves, "A Simultaneous Evaluation of Some Important Cross Sections at 14.7 MeV," Ann. Nucl. Energy **16**, 307 (1989).

[Sol69] M. Soleilhac, J. Frehaut, and J. Gauriau, "Energy Dependence of $\bar{\nu_p}$ for Neutron-Induced Fission of ^{235}U, ^{238}U, and ^{239}Pu from 1.3 to 15 MeV," J. Nucl. Energy **23**, 257 (1969).

[Von90] H. Vonach, A. Pavlik, and B. Strohmaier, "Accurate Determination of $(n, 2n)$ Cross Sections for Heavy Nuclei from Neutron Production Spectra," Nucl. Sci. Eng. **106**, 409 (1990).

[Wag90] M. Wagner *et al.*, "Evaluation of Cross Sections for 14 Important Neutron-Dosimetry Reactions," Physics Data **13-5** (1990).

[Wan89] X. Y. Wang *et al.*, EXFOR data base entry 30935 at http://www.nndc.bnl.gov/nndc/exfor/.

[Wei40] V. F. Weisskopf and D. H. Ewing, Phys. Rev. **57**, 472 (1940).

[Won72] C. Wong *et al.*, "Livermore Pulsed Sphere Program: Program Summary Through July 1971," UCRL-51144, Rev. 2 (1972).

[You00] W. Younes *et al.*, "The ^{235}U(n,2nγ) Yrast Partial Gamma-Ray Cros Sections: A Report on the 1998 and 1999 GEANIE Data and Analysis Techniques," UCRL-ID-140313 (2000).

[You91] P. G. Young and E. D. Arthur, "Theoretical Analyses of (n, xn) Reactions on ^{235}U, ^{238}U, ^{237}Np, and ^{239}Pu for ENDF/B-VI," LA-UR–91-1424 (1991); see also E. D. Arthur *et al.*, "Evaluation and Testing of n+^{239}Pu Nuclear Data for Revision 2 of ENDF/B-V," Nucl. Sci. Eng. **88**, 56 (1984).